

# Real-Time Dynamic $N - 1$ Screening: Identifying High-Risk Lines and Transformers After Common Faults

Ayrton Almada <sup>\*†</sup>, Laurent Pagnier <sup>\*</sup>, Igal Goldshtain <sup>‡</sup>, Saif R. Kazi <sup>†</sup>, and Michael (Misha) Chertkov <sup>\*</sup>

<sup>\*</sup> Program in Applied Mathematics and Department of Mathematics,

University of Arizona, Tucson, AZ 85721, USA

<sup>†</sup> Applied Mathematics and Plasma Physics,

Los Alamos National Laboratory, Los Alamos, NM 87519, USA

<sup>‡</sup> NOGA, Power System Operator of Israel, Haifa, Israel

**Abstract**—Power system operators routinely perform  $N - 1$  contingency analysis, yet conventional tools provide limited guidance on which lines or transformers deserve heightened attention during fast post-fault transients. In particular, static screening does not reveal whether (i) the same faulted line repeatedly triggers severe downstream overloads, or (ii) a specific transformer emerges as vulnerable across many distinct fault scenarios. This paper introduces a real-time dynamic  $N - 1$  screening framework that addresses this gap by estimating, for each counterfactual single-phase transmission fault, the probability of transient over-current on critical grid elements. The output is an operator-facing dashboard that ranks (a) faulted lines whose outages most frequently lead to dangerous transformer overloads, and (b) transformers that consistently overload across top-risk scenarios – both of which are actionable indicators for real-time situational awareness. The approach models post-fault electromechanical dynamics using a linear stochastic formulation of the swing equations with short-lived, fault-localized uncertainty, and combines analytic transient evaluation with cross-entropy-based importance sampling to efficiently estimate rare but high-impact events. All  $N - 1$  contingencies are evaluated in parallel with linear computational complexity. The framework is demonstrated on the IEEE 118-bus system, where it reveals latent high-risk lines and transformers that remain invisible under deterministic dynamic or static  $N - 1$  analysis. Results show orders-of-magnitude computational speedup relative to brute-force Monte Carlo, enabling practical deployment within real-time operational cycles.

**Index Terms**—Importance Sampling, Instantons for Rare Impactful Events, N-1 Contingencies, Power System Dynamics under Faults, Fluctuations, Transmission Grids.

## I. INTRODUCTION

### A. Motivation

Power-system stability is concerned with the ability of the grid to regain an acceptable operating state after disturbances without loss of synchronism or cascading failures. Of particular relevance is transient stability, which governs the short post-fault interval where electromechanical dynamics, protection actions, and topology changes interact most strongly [1]. Increasing heterogeneity and uncertainty in modern grids motivate real-time dynamic security assessment as a complement to traditional offline studies [2]. Recent large-scale events demonstrate that fast fault-driven interactions can trigger low-probability, high-impact outcomes that static screening fails to capture [3], [4].

From an operator’s perspective, not all  $N - 1$  contingencies are equally informative. If a particular transmission line – when faulted – repeatedly appears among the highest-risk scenarios leading to transformer overcurrent, that line deserves increased operational scrutiny, even if it is not traditionally classified as critical. Likewise, assets – and especially transformers – that systematically accumulate post-fault stress become natural targets for monitoring and preventive control.

This work develops an online decision-support framework that quantifies, in probabilistic terms, the risk associated with counterfactual transmission faults. We focus on single-phase disturbances and on the likelihood of secondary effects during the seconds-long post-fault transient, such as overloads of critical equipment, e.g. transformers. Building on [5], which employs a deterministic linear swing model, we introduce fault-induced dynamic uncertainty by modeling short-lived, localized fluctuations in the parameters of the faulted line<sup>1</sup>. The approach is demonstrated on the IEEE 118-bus model of the American Electric Power (AEP) system, aiming at scalable probabilistic transient security assessment for large transmission networks.

The work at UA was supported by (a) NSF DMS-2229012: "Collaborative Research: AMPS: Rare Events in Power Systems: Novel Mathematics, Statistics and Algorithms"; (b) subcontract from NOGA on "Uncertainty-Aware Toolbox for Simulation, Optimization, Control and Planning of Inter Connected Gas and Power Systems". AA was supported by LANL as a graduate research assistant. We are thankful to Prof. J. Blanchet (Stanford) and his team for multiple discussions and consultations on the application of the adaptive importance sampling (cross-entropy) method; and Dr. Bent (LANL) for multiple comments and suggestions.

<sup>1</sup>Fault-induced (co-occurring) uncertainty refers to transient, localized variability during a fault, distinct from ambient system-wide noise.

## B. Main Contributions

This work introduces the following contributions:

- **Efficient  $N - 1$  dynamic screening methodology** — a scalable approach to analyze ensembles of transient responses associated with counterfactual faults on any transmission line, conditioned on a given operating state. Fig. (1) illustrates an example of undesirable transient behavior triggered by a 0.5s line fault.
- **Probabilistic risk framework** — a stochastic modeling and estimation framework that characterizes the temporal evolution of system overloads driven by phase-angle dynamics, enabling quantitative assessment of grid reliability under fault-induced uncertainty.

### Operator View — What this tool provides

For a given operating state, the proposed dynamic  $N - 1$  screening answers three operator-relevant questions in real time:

- **Which faulted transmission lines** most frequently trigger dangerous post-fault overloads elsewhere in the grid.
- **Which transformers or critical lines** repeatedly appear overloaded across the top-ranked fault scenarios.
- **How likely** these overloads are to occur during the first seconds following fault clearance.

This information enables operators to focus attention on specific lines or transformers during stressed conditions, even when those elements are not flagged as critical by conventional  $N - 1$  analysis.

The proposed approach achieves a **three-orders-of-magnitude** (i.e.,  $\sim 10^3$ ) computational efficiency gain over direct Monte Carlo evaluation of counterfactual contingencies through two complementary advances:

- 1) **Analytic reduction:** replacement of time-domain fault simulations by evaluations — via closed-form solutions of linear stochastic swing-equation models incorporating co-occurring and co-located with the faults uncertainty.
- 2) **Targeted sampling:** use of cross-entropy-based importance sampling to focus computational effort on low-probability but highest-impact contingency scenarios.

## C. Outline

The remainder of this paper is organized as follows (Sections III–VIII):

- **System and Fault Modeling** [Section III]:

We develop a scalable linearized second-order stochastic model of transmission-level dynamics based on the swing equations, explicitly incorporating co-occurring noise localized on the faulted line(s). Single-phase transmission faults are modeled over three regimes—pre-fault, fault-on, and post-clearing—capturing both deterministic and stochastic transient effects.

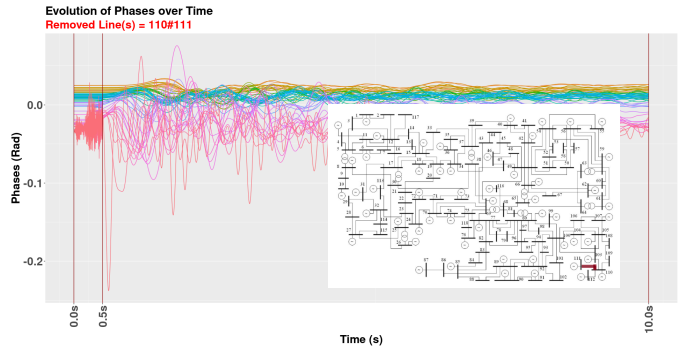


**Fig. 1:** Example of a single-phase transmission fault whose post-clearing transient leads to severe downstream stress. While the faulted line is re-energized, secondary overloads on other elements may persist —motivating the need for dynamic  $N - 1$  screening beyond static criteria.

- **Overload Indicator** [Section IV]:

We introduce a continuous overload indicator that quantifies fault severity by combining thermal limits, fault duration, and phase-angle oscillations, enabling a time-resolved assessment of transient system stress.

- **Scalable Dynamic Evaluation** [Section V]:

We derive analytic and semi-analytic reductions of the governing dynamics that enable efficient re-evaluation of fault-induced transients across large ensembles of counterfactual contingencies.

- **Probabilistic Risk Estimation** [Section VI]:

We estimate rare-event probabilities using Monte Carlo techniques and an efficient Cross-Entropy-based importance sampling method, validated against brute-force MCMC, and implemented within our custom simulator, **N1Plus**.

- **Case Study: IEEE 118-Bus System** [Section VII]:

The proposed framework is evaluated on the IEEE 118-bus test system (118 buses, 177 lines, 19 generators, 9 transformers, and 91 loads), demonstrating accuracy and computational scalability across a range of fault scenarios.

- **Conclusion and Outlook** [Section VIII]:

We summarize the main findings and discuss extensions to larger and more heterogeneous grids, including the integration of data-driven and AI-assisted tools to further scale the methodology.

The overall structure and computational pipeline of the proposed approach are illustrated in Fig. (2):

## II. RELATED WORK AND BACKGROUND

### A. $N - 1$ Contingency Analysis

$N - 1$  contingency analysis<sup>2</sup> is a cornerstone of power-system reliability assessment, requiring the grid to remain stable and within operational limits following the loss of

<sup>2</sup>The proposed methodology also extends to broader contingency classes, including scenarios derived from historical fault data rather than strict  $N - 1$  rules.

## N-1 Plus Pipeline – to Monitor Dynamic N-1 Contingencies

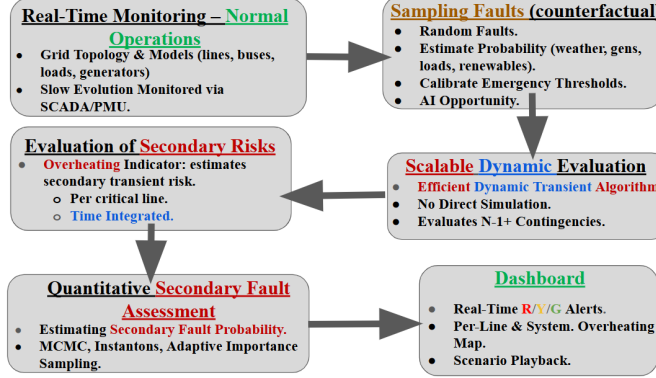


Fig. 2: Conceptual Dashboard for Dynamic Contingency Screening.

any single critical component. This criterion underpins operational standards adopted by organizations such as NERC and ENTSO-E [6]. Conventional  $N-1$  studies rely on static power-flow simulations to identify limit violations and rank contingencies for corrective actions [7]<sup>3</sup>. While effective in steady-state analysis, such approaches are computationally intensive and largely insensitive to transient dynamics, particularly in large, low-inertia systems with high renewable penetration. To address these limitations, we propose a framework for real-time screening of *dynamic N-1 contingencies* that explicitly targets short-term post-fault behavior (sub-second to tens-of-seconds; see Table I). Focusing on common disturbances such as single-phase short circuits<sup>4</sup>, the framework estimates the probability of secondary effects – specifically, transient but severe overloads on critical transmission elements – that may precipitate further instability in stressed operating conditions. The objective is to provide operators with a concise, probabilistic dashboard that enhances situational awareness of rare yet consequential post-fault risks, including line tripping driven by transient overcurrent events.

### B. Rare Event/Instanton Sampling

Rare-event (instanton) methods provide an efficient framework for identifying low-probability, high-impact events in complex systems [8], [9], [10], [11], [12], [13], [14], including power grids [15], [16], [17], [18], [19]. Unlike standard Monte Carlo, these approaches leverage large-deviation theory to characterize the most probable rare trajectories – *instantons* – that drive extreme outcomes such as blackouts and cascading failures [15], [18]. The instanton minimizes a stochastic action (Freidlin–Wentzell) and thereby reveals both the physical mechanism and the exponential scaling of the associated probabilities [8], [12], [14]. Adaptive importance sampling (AIS), and in particular the cross-entropy (CE) method [20], [21], can be interpreted as using instanton-informed proposal

<sup>3</sup>Voltage regulation and dispatch corrections are not considered in this work.

<sup>4</sup>This paper focuses exclusively on single-phase transmission-line faults, which account for the majority of real-world events. Three-phase faults are intentionally excluded to maintain a tight operational scope and avoid conflating distinct protection and dynamic regimes.

families to bias sampling toward the most relevant regions of state space; iterative CE/AIS updates refine this bias via stochastic optimization, yielding substantial variance reduction and, in the low-probability regime, asymptotically optimal (near zero-variance) estimators [20], [21], [9], [13], [22].

## III. DYNAMICS, FAULTS AND OVERLOADS

This section introduces the core modeling framework used throughout the paper: a transmission-level power grid dynamics model based on swing equations. We begin by formulating the system's behavior under small-to-moderate disturbances, then describe how line faults are incorporated into the model, and finally define a safety domain that encodes grid element overload constraints. This framework enables both theoretical analysis and efficient numerical simulation of dynamic contingencies.

### A. Modeling with Swing Equations

We model the transmission network as a collection of generators, loads, and transmission lines operating on multiple time scales. While aggregated load dynamics typically evolve over minutes or longer, generator electromechanical dynamics respond on sub-second to tens-of-seconds horizons. This faster regime governs transient stability and is the focus of the present analysis.

Each bus  $i \in \mathcal{V}$  is associated with a complex voltage  $v_i = V_i e^{j\theta_i}$ , where  $V_i$  denotes the voltage magnitude and  $\theta_i$  the phase angle. Although transmission systems are inherently three-phase, we adopt the standard balanced-network assumption and represent each line by a single equivalent phase [23]. The grid is modeled as an undirected graph  $\mathcal{G} = (\mathcal{V}, \mathcal{E})$ , where  $\mathcal{V}$  denotes the set of buses and  $\mathcal{E}$  the set of transmission lines. We assume a lossless network with constant voltage magnitudes, which is appropriate over the short time scales considered.

Following [5], system dynamics are described by the linearized swing equations

$$m_i \ddot{\theta}_i + d_i \dot{\theta}_i + \sum_{\{i,j\} \in \mathcal{E}} \beta_{ij} (\theta_i - \theta_j) = p_i, \quad i \in \mathcal{V}, \quad (1)$$

where  $m_i$  and  $d_i$  denote inertia and damping coefficients,  $p_i$  represents net power injection, and  $\beta_{ij} = V_i V_j B_{ij}$  is the effective stiffness of line  $\{i,j\}$ . In vector form,

$$M \ddot{\theta} + D \dot{\theta} + L \theta = p, \quad (2)$$

with diagonal inertia and damping matrices  $M$  and  $D$ , and weighted graph Laplacian  $L = (L_{ij})$  defined by

$$L_{ij} = \begin{cases} \sum_{k \in \mathcal{V}} \beta_{ik}, & i = j, \\ -\beta_{ij}, & i \neq j. \end{cases}$$

Eq. (2) should be interpreted as a linearization of more general seconds-scale dynamics around a pre-disturbance operating point. During fault events, the parameters  $\beta_{ij}$  associated with the affected line may change partially or completely, altering the network Laplacian and driving transient behavior. The modeling of these fault-induced variations is addressed in the following subsection.

TABLE I: N-1 Analysis vs Dynamic Evaluation.

Aspect	N-1 Contingency	Swing Equations
Objective	Secure post-fault	Assess transient stability
Time Scale [s]	$10^0 - 10^2$	$10^{-3} - 10^0$
Application	Operations and planning	Dynamic stability studies
Model	AC/DC power flow	Generator and load responses as ODEs

### B. Effect of Co-Occurring Noise

Transmission faults are not clean events. On the contrary they are noisy. During the fault various electrical parameters vary abruptly due to arcing, intermittent grounding, and protection or reclosing actions. These variations/disturbances are transient, state-dependent, and confined to the faulted location. We refer to these disturbances as **co-occurring noise on the faulty line** [24], [25]. As detailed in the next subsection we model the co-occurring noise as an addition to the susceptance of the faulted line – a short-lived but stochastic contribution. This produces localized multiplicative noise entering the linearized swing equations through the network Laplacian. The model retains analytical tractability while capturing amplification of the fault-induced uncertainty; its detailed formulation is given in Section V.

### C. Simulating Faults

We consider faults occurring exclusively on transmission lines; faults at buses (e.g., generators or transformers) are excluded, although the framework readily extends to these cases. Fault occurrences are modeled as a Poisson process with line-dependent rates that may vary slowly with operating conditions. In this work, we focus on **single-phase-to-ground faults**, which constitute the dominant class of transmission disturbances [26].

Under standard operating rules, the remaining two phases may continue to operate during a single-phase fault until clearance, typically within one second. Adopting a balanced-network approximation, a single-phase fault of duration  $\tau$  is modeled by a temporary reduction of the affected line's susceptance from  $\beta_{ij}$  to  $\frac{2}{3}\beta_{ij}$ , reflecting reduced transfer capability; upon clearance, the susceptance is restored to its nominal value<sup>5</sup>. The fault duration  $\tau$  may be treated as deterministic or stochastic (e.g., exponentially distributed), depending on protection settings.

Conditioned on a fault of duration  $\tau$ , the susceptance of the faulted line is modeled as

$$\beta_{ij}(t) = \overline{\beta_{ij}}(t) + \sigma_{ij}\zeta(t)\mathbb{I}(t \in [0, \tau]), \quad (3)$$

where  $\zeta(t)$  denotes unit white noise,  $\overline{\beta_{ij}}(t) = \begin{cases} \frac{2}{3}\beta_{ij}, & t \leq \tau, \\ \beta_{ij}, & t > \tau, \end{cases}$  and  $\sigma_{ij}$  quantifies the strength of fault-induced uncertainty (taken here as  $\sigma_{ij} = \beta_{ij}$ ). This formulation captures the three stages of system evolution—**Pre-Fault**, **Fault**, and **Operational** intervals—summarized schematically in Fig. (3).

<sup>5</sup>This approximation neglects millisecond-to-second unbalanced dynamics; more detailed fault representations are left for future work.

### Flowchart of Fault-Induced Transient

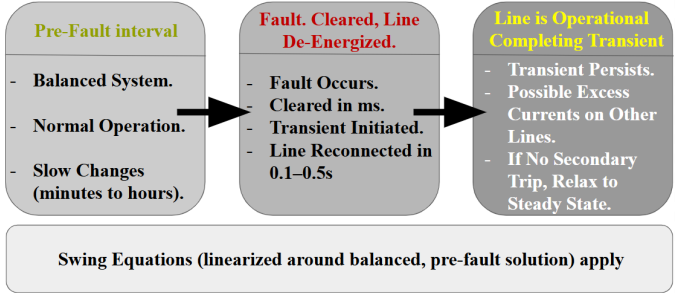


Fig. 3: Fault timeline: system is balanced, pre-fault; fault is cleared, a faulty line is de-energized; line is back in service, post-fault transient.

### D. Safety Polytope

We define the *safety polytope* as the domain of phase configurations that ensure all line flows remain within their respective thermal (or angular) limits. Specifically, it characterizes the set of phase angles for which the power transmitted along every line does not exceed its safety threshold:

$$\Pi_{\theta} \doteq \left\{ \theta \in [-\pi, \pi]^{|\mathcal{V}|} \mid \forall \{i, j\} \in \mathcal{E} : |\beta_{ij}(\theta_i - \theta_j)| \leq \bar{p}_{ij} \right\},$$

where  $\bar{p}_{ij}$  denotes the maximum allowable phase difference across line  $\{i, j\}$ , which indirectly encodes the corresponding thermal or stability constraint on power flow. The set  $\Pi_{\theta}$  thus models the domain of safe operations for the system under the linearized swing approximation.

### IV. OVERLOAD INDICATOR

To quantify **transient line stress**, we define an *overload indicator* based on the solution of the linearized stochastic swing eqs. (6). Let  $\theta(t) = (\theta_i(t) \mid i \in \mathcal{V})$  denote the phase angles over  $t \in [0, T]$ , and let  $\beta_{ij}(t)$  be the time-varying susceptance of line  $\{i, j\}$  (Eq. (3)). For a monitored line  $\{i, j\} \in \mathcal{E}$ , the **line-specific overload indicator** is

$$S_{ij}(\theta_{0 \rightarrow T}) \doteq \int_0^T \mathbb{I}(|\beta_{ij}(t)(\theta_i(t) - \theta_j(t))| > \bar{p}_{ij}) dt, \quad (4)$$

where  $\bar{p}_{ij}$  is a safety threshold associated with the line's thermal limit and  $\mathbb{I}(\cdot)$  is the indicator function. The monitored line need not coincide with the faulted line; overloads may be induced anywhere in the network by a given fault. To assess system-wide impact, we also define the **global overload indicator** across a set of monitored lines  $\mathcal{E}_m \subseteq \mathcal{E}$ :

$$S(\theta_{0 \rightarrow T}) \doteq \sum_{\{i, j\} \in \mathcal{E}_m} S_{ij}(\theta_{0 \rightarrow T}), \quad (5)$$

with  $\theta_{0 \rightarrow T} \doteq (\theta_i(t) \mid i \in \mathcal{V}, t \in [0, T])$ . The quantity  $S(\theta_{0 \rightarrow T})$  accumulates the duration of overloads across monitored lines; since the integrand in (4) is binary, the indicator increases in discrete steps, capturing both the number of affected lines and the time spent above limits.

The random variables  $S_{ij}(\theta_{0 \rightarrow T})$  and  $S(\theta_{0 \rightarrow T})$  serve as the primary risk metrics. Their distributions over ensembles of fault realizations and operating conditions are used to assess transient vulnerability and estimate overload probabilities.

## V. SCALABLE DYNAMIC EVALUATION

Linear swing Eqs. (1,2) describing dynamics of phases over grids under co-occurring noise Eq. (3) from time 0 when the fault occurred and line (phase) was de-energized, through the period of time  $\tau$  when the line was back in service, but swings of the phase dynamics continue, and all the way till time  $T$  after the fault when the transient stabilized, can be restated in the following compact form for  $t \in [0, T]$ :

$$\begin{aligned} d\mathbf{x} &= (\bar{A}(t) \mathbf{x} + \mathbf{P}) dt + \mathbb{I}(t \in [0, \tau]) G_{ij} x dW(t), \quad (6) \\ G_{ij} &= \begin{bmatrix} \mathbb{O}_{n \times n} & \sigma_{ij} \mathbf{M}^{-1} [e_i - e_j] \cdot [e_i - e_j]^T \\ \mathbb{O}_{n \times n} & \mathbb{O}_{n \times n} \end{bmatrix}, \\ \mathbf{P} &\doteq \begin{pmatrix} \mathbf{p} \\ \mathbf{0} \end{pmatrix}, \quad \mathbf{x} \doteq \begin{pmatrix} \dot{\theta}(t) \\ \theta(t) \end{pmatrix}, \quad \mathbf{x}_0 \doteq \begin{pmatrix} \mathbf{0} \\ \mathbf{L}_0^{-1} \mathbf{p} \end{pmatrix}, \\ \bar{A}(t) &= \begin{bmatrix} \mathbf{M}^{-1} \mathbf{D} & \mathbf{M}^{-1} \bar{L}(t) \\ \mathbb{O}_{n \times n} & \mathbb{1}_{n \times n} \end{bmatrix} = \mathbf{A}_0 + \mathbb{I}(t \in [0, \tau]) \delta \mathbf{A}. \end{aligned}$$

where  $G_{ij}$  is the noise structure matrix associated to the removed line  $\{i, j\} \in \mathcal{E}$  and  $dW(t)$  is a Wiener process.

In order to save the space we do not present explicit expressions for: the diagonal matrices  $\mathbf{M}$  and  $\mathbf{D}$  – represent inertia and damping; pre- and post-fault value  $\mathbf{A}_0$  and its on-fault correction  $\delta \mathbf{A}$  are due to the varying susceptance of the faulty line. Eq. (6) is a **linear stochastic differential equation with multiplicative nilpotent noise** [27].

Solution of (6) is explicitly given by

$$\begin{aligned} \mathbf{x}(t) &= \Phi(t, 0) \mathbf{x}_0 + \int_0^t \Phi(t, s) \mathbf{P} ds, \quad \forall t \leq \tau, \\ \mathbf{x}(t) &= e^{\mathbf{A}_0(t-\tau)} \mathbf{x}_\tau + \int_\tau^t e^{\mathbf{A}_0(t-t_1)} \mathbf{P} dt_1, \quad \forall t > \tau. \end{aligned} \quad (7)$$

Where

$$\begin{aligned} \Phi(t, s) &= \exp \left( \left( \tilde{A} - \frac{1}{2} G_{ij}^2 \right) (t - s) + G_{ij} (W(t) - W(s)) \right) \\ &= \exp \left( \tilde{A}(t - s) \right) (\mathbb{1}_{2n \times 2n} + G_{ij} (W(t) - W(s))) \end{aligned}$$

is the fundamental matrix [28], [29] used to solve the stochastic portion of Eq. (6) and  $\tilde{A} = \mathbf{A}_0 + \delta \mathbf{A}$ . Eq. (7) must usually be solved numerically. However, assuming that the initial condition  $\mathbf{x}(t_0)$  and the eigendecompositions  $\mathbf{A} = \mathbf{U} \Lambda \mathbf{U}^{-1}$ ,  $\tilde{A} = \tilde{\mathbf{U}} \Lambda \tilde{\mathbf{U}}^{-1}$ , with  $\mathbf{U} \mathbf{U}^{-1} = \tilde{\mathbf{U}} \tilde{\mathbf{U}}^{-1} = \mathbb{I}$ , are known, the system dynamics is governed by

$$\begin{aligned} d\boldsymbol{\xi} &= (\boldsymbol{\Lambda} \boldsymbol{\xi} + \mathbf{U}^{-1} \mathbf{P}) dt + \mathbf{U}^{-1} G_{ij} \boldsymbol{\xi} dW(t), \quad \forall t \leq \tau, \\ \dot{\boldsymbol{\xi}} &= \tilde{\boldsymbol{\Lambda}} \boldsymbol{\xi} + \tilde{\mathbf{U}}^{-1} \mathbf{P}, \quad \forall t > \tau, \\ \boldsymbol{\xi}_0 &= \mathbf{U}^{-1} \mathbf{x}_0, \end{aligned}$$

This initial value problem can be solved analytically for the eigenmodes  $\boldsymbol{\xi}$ , then converted into  $\mathbf{x}$  as  $\mathbf{x}(t) = \tilde{\mathbf{U}} \boldsymbol{\xi}(t)$ ,  $t \leq \tau$  and  $\mathbf{x}(t) = \mathbf{U} \boldsymbol{\xi}(t)$ ,  $t > \tau$ , where tilde denotes that the is the eigenvectors of the perturbed matrix  $\tilde{\mathbf{A}}$  that are used. More details can be found in [30].

## VI. PROBABILISTIC RISK ASSESSMENT

Assuming all the initial information from Section V, we now focus on estimating the probability of exiting the safety polytope  $\Pi_\theta$  using the overload indicator  $S(\theta_{0 \rightarrow T})$  and an efficient sampling. Let  $x_{0 \rightarrow T}^{(0)} = x(0 \rightarrow T)$  be the trajectory of the solution of the initial value problem stated in Eq. (6) and  $S_{ij}(\theta_{0 \rightarrow T}^{(0)})$  be the line-specific overload indicator of  $x_{0 \rightarrow T}^{(0)}$  for all  $\{i, j\} \in \mathcal{E}$ :

$$S_{ij}(\theta_{0 \rightarrow T}^{(0)}) = \int \mathbb{I} \left( \left| \beta_{ij}(t) \left( \theta_i^{(0)}(t) - \theta_j^{(0)}(t) \right) \right| > \bar{p}_{ij} \right) dt. \quad (8)$$

We estimate the probability  $Q_{ij} = \mathbb{P}[S_{ij}(\theta_{0 \rightarrow T}) \geq \gamma] = \mathbb{E}[\mathbb{I}_{\{S_{ij}(\theta_{0 \rightarrow T}) \geq \gamma\}}]$  for a fixed threshold  $\gamma > 0$ , i.e. **the likelihood of overloading line  $\{i, j\} \in \mathcal{E}$  for more than  $\gamma$  seconds**. An efficient and accurate way to approximate  $Q_{ij}$  is by using **adaptive importance sampling** via the **cross entropy method** [20], [21], we briefly explain how does this work and how do we implement it for this particular case:

### A. Cross-Entropy Method (CEM)

CEM [20], [21] adaptively fits an importance law to concentrate samples in the rare-event region

$$\mathcal{R}_\gamma = \{Z = (\alpha, \tau) \in (\{\emptyset\} \cup \mathcal{E}) \times \mathbb{R}_+ \mid S_{ij}(\theta_{0 \rightarrow T}) \geq \gamma\}.$$

We model via a simple parametric family characterized by the sampling density:  $q_\nu(\alpha, \tau) = \phi_\alpha \text{Pois}(\tau; \lambda_\alpha)$ , where  $\phi_\alpha \geq 0$ ,  $\alpha \in \mathcal{E}$ ,  $\sum_{\alpha \in \mathcal{E}} \phi_\alpha = 1$ ,  $\tau \in \mathbb{R}_+$  and with the parameter  $\nu \doteq (\phi_\alpha, \lambda_\alpha \mid \alpha \in \mathcal{E})$ . Starting from  $\nu^{(0)}$ , at iteration  $t$  we draw  $Z_k \sim q_{\nu^{(t-1)}}$  samples, compute trajectories  $\theta_{0 \rightarrow T}^{(k)}$  and importance weights

$$w_k \propto \mathbf{1}\{S_{ij}(\theta_{0 \rightarrow T}^{(k)}) \geq \gamma\} \frac{p_Z(Z_k)}{q_{\nu^{(t-1)}}(Z_k)}$$

also restricting to an “elite” subset.

The CE update maximizes the weighted log-likelihood. Iterating until stabilization gives  $q_Z^* = q_{\nu^*}$ . The IS estimator of  $Q_{ij} = \mathbb{P}_{p_Z}[S_{ij}(\theta_{0 \rightarrow T}) \geq \gamma]$  is

$$\hat{Q}_{ij} = \frac{1}{N} \sum_{k=1}^N \mathbf{1}\{S_{ij}(\theta_{0 \rightarrow T}^{(k)}) \geq \gamma\} \frac{p_Z(\alpha_k, \tau_k)}{q_Z^*(\alpha_k, \tau_k)}, \quad (\alpha_k, \tau_k) \sim q_Z^*.$$

### B. N1Plus

We introduce N1Plus, a computational engine designed to efficiently simulate the dynamic response of transmission power grids to fault events, capturing system behavior across sub-second to minute timescales. The model perturbs parameters in a linearized form of the swing equations, keeping them fixed prior to transient stabilization. Fault events are sampled, and the resulting system dynamics are resolved analytically

using the closed-form solutions in Eqs. (7), avoiding full nonlinear simulations. Based on these simulations, N1Plus estimates the probability of exiting the safety polytope  $\Pi_\theta$  through the cumulative overload indicator  $S(\theta_{0 \rightarrow T})$ , as well as line-specific indicators that identify critical network components. To evaluate the probability of extreme events, stochastic sampling techniques are used to approximate the distribution of line overloads triggered by random disturbances. This framework represents a dynamic and stochastic generalization of the classical  $N - 1$  contingency analysis, providing a novel tool for operational resilience assessment. Conceptually, it extends the static instanton methodology proposed in [16] and builds upon the rare-event sampling techniques developed in [19]. The methodology underlying N1Plus is summarized in Algorithm 1.

---

**Algorithm 1** N1Plus Dynamic Kernel (pseudo-code)

---

**Require:**  $\mathcal{G} = (\mathcal{V}, \mathcal{E}), L, M, D, P, \Pi_\theta$  (Section V),  $\lambda \in [0.1, 0.9]$  rate of fault's duration,  $T > 0$  duration of simulation,  $N > 0$  sample size,  $\gamma \geq 0$  threshold, parametric family  $q_Z(\cdot; \nu)$  with initial parameters  $\nu^{(0)}$ .

- 1: Initialize iteration counter  $t \leftarrow 0$ .
- 2: **repeat**
- 3:    $t \leftarrow t + 1$
- 4:   **for**  $i = 1, \dots, N$  **do**
- 5:      $(\alpha_i, \tau_i) \sim q_Z(\cdot; \nu^{(t-1)})$   $\triangleright$  Fault dur.+tripped line.
- 6:     Solve (6) for  $(\alpha_i, \tau_i)$ :  $\theta_{0 \rightarrow T}^{(i)}$   $\triangleright$  Use (7).
- 7:      $S_i \leftarrow S(\theta_{0 \rightarrow T}^{(i)})$   $\triangleright$  Use (5).
- 8:   **end for**
- 9:    $E^{(t)} = \{(\alpha_i, \tau_i) : S_i \geq \gamma^{(t)}\}$   $\triangleright$  Elite set.
- 10:    $\gamma^{(t)} : (1 - \rho)$ -quantile of  $\{S_i\}$   $\triangleright \rho \in (0, 1)$ .
- 11:    $\nu^{(t)} = \underset{\nu}{\operatorname{argmax}} \left\{ \sum_{(\alpha_i, \tau_i) \in E^{(t)}} \log(q_Z(\alpha_i, \tau_i; \nu)) \right\}$
- 12: **until** Convergence of  $\nu^{(t)}$ : optimal distribution  $q_Z^*(\cdot; \nu^{(t)})$ .
- 13: Draw  $\{(\alpha_k, \tau_k) \sim q_Z^*\}_{k=1}^N$  from  $q_Z^*(\cdot; \nu^{(t)})$ .
- 14: For each  $(\alpha_k, \tau_k)$ , solve (6) and compute  $S_{lm}(\theta_{0 \rightarrow T}^{(k)})$ .
- 15: Estimate  $\hat{Q}_{lm}$   $\triangleright$  Use (VI-A).
- 16: **return**  $\hat{Q} \doteq \left( \hat{Q}_{lm} \right)_{\{l, m\} \in \mathcal{E}}$   $\triangleright$  Repeat 14-15  $\forall \{l, m\} \in \mathcal{E}$ .

---

## VII. CASE STUDY: IEEE 118-BUS SYSTEM

We evaluate the proposed framework by applying the **N1Plus Algorithm 1** to the IEEE 118-bus test system, which comprises 118 buses, 19 generators, 35 synchronous condensers, 177 transmission lines, 9 transformers, and 91 loads. The system model and parameters required by Algorithm 1 and Section V are taken from [31]. Our assessment focuses on both the accuracy and computational efficiency of the proposed approach. The final implementation will be released as an open-source Julia package, **N1Plus.jl**. Numerical results for single-phase fault scenarios with stochastic perturbations are reported in Section VII-A. For each faulted line  $\{i, j\}$ , we analyze the statistical behavior of the overload indicator

$S_{ij}(\theta_{0 \rightarrow T})$  as a function of the random fault duration  $\tau$ , and estimate  $Q_{ij}(\tau) = \mathbb{P}[S_{ij} \geq T^{(*)}]$ , which quantifies the probability that the overload indicator exceeds a prescribed threshold  $T^{(*)}$ . For single-phase faults, we set  $T^{(*)} = 1$  s. To aid interpretation, we adopt a qualitative risk classification based on  $Q_{ij}$ : values exceeding 4% are labeled red (critical risk), values between 2.5% and 4% are labeled yellow (moderate risk), and values below 2.5% are labeled green (low risk). To isolate and visualize the impact of fault-induced uncertainty, we perform a comparative analysis following the methodology of [5]. Section VII-B reports results for single-phase faults in the absence of multiplicative noise, corresponding to the deterministic swing-equation model

$$\begin{aligned} \dot{\mathbf{x}} &= \mathbf{A}(t)\mathbf{x} + \mathbf{P}, \\ \mathbf{P} &\doteq \begin{pmatrix} \mathbf{p} \\ \mathbf{0} \end{pmatrix}, \quad \mathbf{x} \doteq \begin{pmatrix} \dot{\theta}(t) \\ \theta(t) \end{pmatrix}, \quad \mathbf{x}_0 \doteq \begin{pmatrix} \mathbf{0} \\ \mathbf{L}_0^{-1}\mathbf{p} \end{pmatrix}, \\ \mathbf{A}(t) &= \begin{bmatrix} \mathbf{M}^{-1}\mathbf{D} & \mathbf{M}^{-1}\mathbf{L}(t) \\ \mathbb{O}_{n \times n} & \mathbb{1}_{n \times n} \end{bmatrix} = \mathbf{A}_0 + \mathbb{I}(t \in [0, \tau]) \delta \mathbf{A}. \end{aligned} \quad (9)$$

The same threshold  $T^{(*)} = 1$  s and risk classification are used for consistency. These thresholds are illustrative and are not intended to represent operational limits; in practice, such values should be specified by system operators based on empirical data and engineering judgment.

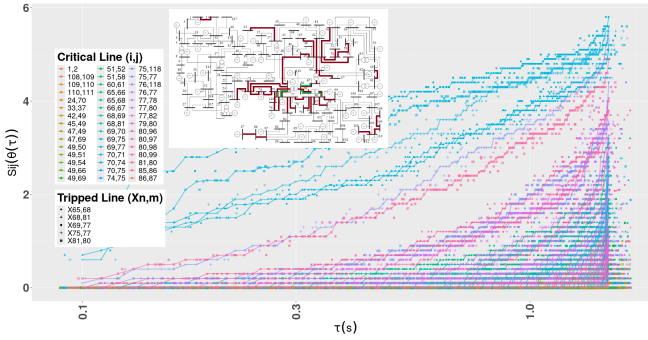
### A. Statistics of the Single Phase Fault with $T^{(*)} = 1$ s

Figs. (4a) and (5a) present the results obtained from a total of  $N = 100,000$  simulations of system of Eqs. (6). In these simulations, each fault corresponds to a partial removal of a transmission line (line's susceptance is set to  $\frac{2}{3}$  of its nominal value during fault). The tripped line in each sample is selected uniformly at random from all lines in the grid, and the fault duration is drawn from an exponential distribution with rate parameter  $\lambda = 0.1$ . As illustrated in Fig. (4a), a total of **3 relevant transmission lines**  $\{\{69, 77\}, \{81, 80\}, \{75, 77\}\} \in \mathcal{E}^6$  exhibit sustained overload levels  $S_{ij}(\theta(\tau)) > 1$  for fault durations  $\tau \geq 0.8$  s. This regime corresponds to a **worst-case operating scenario**. As shown in Fig. (5a), for these **critical lines** the probability of overheating enters the **Emergency Zone**, with  $\mathbb{P}[S_{ij} \geq T^{(*)}] > 4\%$ , whenever the fault duration satisfies  $\tau > 0.8$  s.

### B. Statistics of the Single Phase Fault with $T^{(*)} = 1$ s and no noise in the system

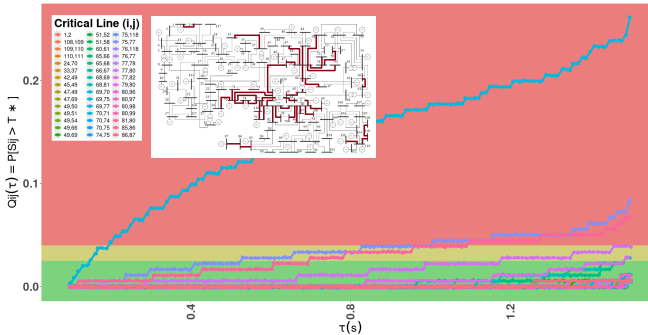
Figs. (4b) and (5b) present the results obtained from a total of  $N = 100,000$  simulations of the system of Eqs. (9). In this case, each fault corresponds to a partial removal of a transmission line (see Footnote 5). The tripped line in each simulation is selected uniformly at random from all lines in the grid, and the fault duration is drawn from an exponential distribution with rate parameter  $\lambda = 0.1$ . As shown in

<sup>6</sup>**Critical lines**, together with the corresponding **tripped lines**, are highlighted in **red** and **green**, respectively, in the IEEE118-bus network diagram shown in Fig. (4a).



**(a) Overload indicator vs. fault duration (single-phase faults).** Each curve represents the overload of an individual line as a function of the fault duration  $\tau$ . **Tripped lines** ( $X_{n,m}$ ) attain the maximum instantaneous overload, whereas **critical transformer-connected lines** ( $i,j$ ) accumulate the largest total overload. Relevant lines in the IEEE-118 network are highlighted.

**Fig. 4: Overload evolution versus fault duration.** Comparison between stochastic dynamics (SDE, left) and deterministic dynamics (ODE, right).



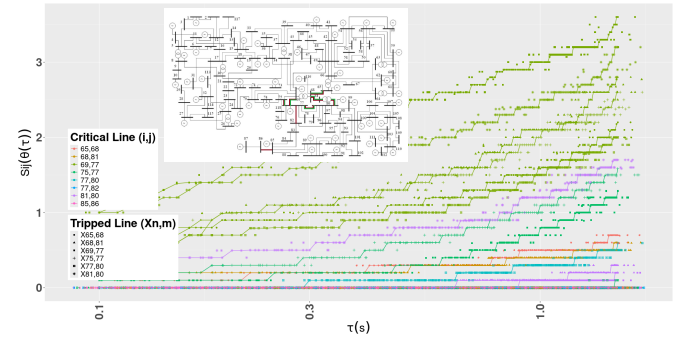
**(a) Probabilistic security assessment (single-phase faults).** For each critical line  $(i,j)$  and fault duration  $\tau$ , the probability  $\mathbb{P}[S_{ij} \geq T^{(*)}]$  is evaluated. Risk classification based on  $Q_{ij}(\tau)$ : **safe** ( $< 0.025$ ), **warning** ( $0.025\text{--}0.04$ ), **emergency** ( $> 0.04$ ).

**Fig. 5: Overload probability versus fault duration.** Comparison between stochastic dynamics (SDE, left) and deterministic dynamics (ODE, right).

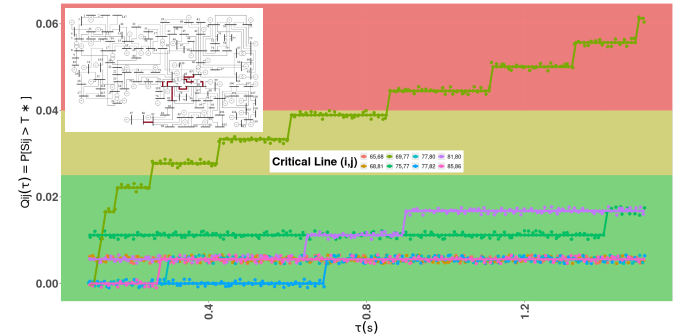
Fig. (4b), one **relevant line**  $\{69, 77\} \in \mathcal{E}$ <sup>7</sup> accumulates a significant overload,  $S_{ij}(\theta(\tau)) > 1$ , for fault durations  $\tau > 0.8$  s. This configuration defines the corresponding **worst-case scenario**. As illustrated in Fig. (5b), only a small subset of these **critical lines** enters the **Emergency Zone**, with overheating probabilities satisfying  $\mathbb{P}[S_{ij} \geq T^{(*)}] > 4\%$  for fault durations  $\tau > 0.8$  s.

A clear contrast emerges between the results reported in Sections VII-A and VII-A. In the stochastic (SDE) setting, a substantially larger number of lines (45) accumulate higher overload levels compared to the deterministic (ODE) case (8). This difference is reflected both in the maximum observed overloads:  $S_{ij}(\theta(\tau)) > 5.5$  in Fig. (4a) versus  $S_{ij}(\theta(\tau)) < 3.5$  in Fig. (4b), and in the resulting risk profiles. In the ODE case, only a single line reaches the **Emergency Zone** threshold, with  $\mathbb{P}[S_{ij} \geq T^{(*)}] \geq 4\%$  (Fig. (5b)), whereas in the SDE case three lines exceed this threshold, triggering **Emergency Zone** alerts at a higher probability level,  $\mathbb{P}[S_{ij} \geq T^{(*)}] \geq 6\%$ .

<sup>7</sup>These **critical lines** are highlighted in red in the IEEE118 diagram shown in Fig. (5b).



**(b) Overload indicator vs. fault duration without multiplicative noise (single-phase faults).** Same definitions and notation as in Fig. 4a.



**(b) Probabilistic security assessment without multiplicative noise (single-phase faults).** Same definitions and notation as in Fig. 5a.

Taken together, these results indicate that explicitly modeling co-occurring noise fundamentally alters the perceived risk landscape. While deterministic dynamics identify only a narrow set of vulnerable components, the stochastic formulation reveals a broader and more severe set of latent failure modes, with higher overload magnitudes and substantially elevated overheating probabilities. This demonstrates that noise-driven excursions during post-fault transients can amplify stress beyond what is predicted by nominal trajectories, underscoring the importance of stochastic dynamic screening for identifying low-probability, high-impact contingencies that would remain invisible to purely deterministic  $N - 1$  analyses [1].

### C. Benchmark Analysis

Tables II and III benchmark the efficiency of estimating the global overload probability using the Cross-Entropy Method (CEM; Section VI-A) for systems with and without multiplicative noise, corresponding to Eqs. (9) and (6), respectively. Following Section VI, we estimate  $Q = \mathbb{P}[S(\theta_{0 \rightarrow T}) \geq \gamma]$  for thresholds  $\gamma \in \{0, 0.5, 5, 10\}$  using sample sizes  $N \in$

**TABLE II:** Processing Time & Convergence Comparison: Cross-Entropy (VI-A) vs. Monte Carlo [32] for global overload (5) probability at thresholds ( $\gamma$ ). **CEM estimate** converges faster (time & sample size) than **MC estimate**.

Cross Entropy Method				Monte Carlo Method		
$\gamma$ [s]	Sample Size	$\hat{Q} \approx \mathbb{P}[S > \gamma]$	Mean Time [s]	Sample Size	$\hat{Q} \approx \mathbb{P}[S > \gamma]$	Mean Time [s]
0	2000	<b>0.242621</b>	$1.905 \times 10^2$	10000	<b>0.24257514</b>	$9.505 \times 10^2$
0.5	3500	<b>0.131398</b>	$3.334 \times 10^2$	25000	<b>0.13137737</b>	$2.375 \times 10^3$
5.0	10000	<b>0.013108</b>	$9.505 \times 10^2$	50000	<b>0.01309973</b>	$4.750 \times 10^3$
10.0	12500	<b>0.002121</b>	$1.188 \times 10^3$	50000	<b>0.00211995</b>	$4.750 \times 10^3$

**TABLE III:** Processing Time & Convergence Comparison: Cross-Entropy (VI-A) vs. Monte Carlo [32] for global overload (5) probability at thresholds ( $\gamma$ ) **with no multiplicative noise in the system**. **CEM estimate** converges faster (time & sample size) than **MC estimate**.

Cross Entropy Method				Monte Carlo Method		
$\gamma$ [s]	Sample Size	$\hat{Q} \approx \mathbb{P}[S > \gamma]$	Mean Time [s]	Sample Size	$\hat{Q} \approx \mathbb{P}[S > \gamma]$	Mean Time [s]
0	2000	<b>0.0806613</b>	$1.905 \times 10^2$	10000	<b>0.08065838</b>	$9.505 \times 10^2$
0.5	3500	<b>0.0337429</b>	$3.334 \times 10^2$	25000	<b>0.03373932</b>	$2.375 \times 10^3$
5.0	10000	<b>0.0000102</b>	$9.505 \times 10^2$	50000	<b>0.00000985</b>	$4.750 \times 10^3$
10.0	12500	<b>0.0000021</b>	$1.188 \times 10^3$	50000	<b>0.00000189</b>	$4.750 \times 10^3$

$\{2000, 3500, 10000, 12500, 25000, 50000\}$ . Each table reports the minimum sample size required for convergence together with the corresponding mean processing time.

Across all thresholds, CEM consistently converges with one to two orders of magnitude fewer samples and substantially lower computational cost than standard Monte Carlo [32], while producing statistically consistent estimates. Moreover, introducing multiplicative (non-ambient) noise significantly increases the estimated overload probabilities at all thresholds, elevating events that are extremely rare in the deterministic setting to non-negligible risk levels. These results underscore the combined importance of variance-reduction techniques and explicit modeling of fault-induced uncertainty: brute-force Monte Carlo becomes impractical for rare-event estimation, while deterministic models systematically underestimate transient overload risk.

## VIII. CONCLUSION AND OUTLOOK

This work develops a *dynamic yet analytically tractable* framework for real-time  $N - 1$  security assessment in transmission-level power systems, with a specific focus on short-term post-fault risk that is not captured by conventional static or deterministic dynamic screening. Starting from a linearized swing-equation formulation, we derive closed-form transient evaluations that replace repeated time-domain simulations with efficient analytical kernels, enabling fast and scalable assessment of large ensembles of counterfactual faults.

Building on this foundation, we introduce an **Overload Indicator** that quantifies the severity and duration of transient over-current events in a risk-consistent manner, and embed it within an efficient rare-event sampling engine – **N1Plus** – designed explicitly for operator-facing decision support. Rather than merely flagging whether a contingency is unsafe, the proposed framework reveals *which faulted lines* most frequently lead to dangerous downstream overloads and *which transformers or corridors* repeatedly emerge as vulnerable across top-ranked scenarios. This recurrence-based perspective

provides actionable guidance on where operator attention should be concentrated during stressed operating conditions.

Validation on the IEEE 118-bus system demonstrates (i) sub-second evaluation times on standard hardware for  $\mathcal{O}(10^5)$  counterfactual fault trajectories, and (ii) close agreement with benchmark simulations, including scenarios involving severe single-phase faults. Importantly, the stochastic formulation reveals a broader and more severe risk landscape than deterministic models, exposing latent vulnerabilities that would remain invisible under traditional  $N - 1$  analysis.

**Next steps and future directions.** Future development of **N1Plus** will focus on shaping the methodology toward multiple complementary use cases:

- 1) **Scalability and sparsity.** Porting the analytical kernels to sparse linear-algebra backends and GPU-accelerated solvers to enable real-time screening of large, multi-area systems ( $n \sim 10^4$  buses) within SCADA/EMS operational cycles.
- 2) **Nonlinear and voltage-coupled dynamics.** Extending the current formulation to include reduced-order voltage, protection, and converter models, allowing the framework to capture minute-scale voltage excursions, relay interactions, and low-inertia phenomena that are not represented in the present model.
- 3) **Data-driven parameter tuning.** Incorporating PMU and SCADA measurements through Bayesian updating and physics-informed priors to enable online calibration of fault statistics, protection clearing times, and fault-induced uncertainty parameters.
- 4) **Uncertainty-aware protection and recovery analysis.** Formalizing notions of system safety, recovery, and resilience via return-time and recurrence distributions under stochastic injections and component-level uncertainty, with direct relevance to protection setting validation.

**Operational, protection, and planning value.** Because **N1Plus** preserves analytical transparency while remaining computationally efficient, it naturally supports multiple modes

of use. In operational settings, it functions as a real-time dashboard that ranks dynamic  $N-1$  contingencies and highlights lines and transformers that warrant heightened attention during post-fault transients. In protection studies, it provides a quantitative framework for evaluating the sensitivity of overload risk to fault duration, relay timing, and uncertainty levels, supporting calibration and stress-testing of protection schemes. In planning and reinforcement studies, it enables systematic ranking of latent vulnerabilities and evaluation of targeted upgrades by estimating the probability of rare but high-impact transient events.

Recent large-scale disturbances – such as the April 2025 Iberian blackout [3] – underscore the limitations of static security metrics when fast electromechanical, voltage, and protection dynamics dominate system behavior. By explicitly modeling transient trajectories and their associated risks, **N1Plus** complements existing tools and helps uncover failure pathways that may remain hidden under conventional analyses. In this way, it bridges the gap between high-fidelity electromagnetic transient simulations, accurate but computationally intensive, and traditional static screening methods, fast but dynamics-blind, offering a practical and extensible approach to transient risk assessment in increasingly low-inertia, renewable-rich power systems.

## REFERENCES

- [1] J. Machowski, Z. Lubosny, J. W. Bialek, and J. R. Bumby, *Power System Dynamics: Stability and Control*. John Wiley & Sons, 2020.
- [2] A. Xue, F. F. Wu, Q. Lu, and S. Mei, “Power system dynamic security region and its approximations,” *IEEE Transactions on Circuits and Systems I: Regular Papers*, 2006.
- [3] ENTSO-E Expert Panel, “Grid incident in spain and portugal on 28 april 2025,” April 2025. Available online.
- [4] FERC, NERC, and Regional Entity Staff, “The february 2021 cold weather outages in texas and the south central united states,” November 2021. Technical report.
- [5] A. Almada *et al.*, “Real-time stochastic assessment of dynamic n-1 grid contingencies,” 2025. arXiv preprint arXiv:2510.18007.
- [6] D. Chatterjee, J. Webb, Q. Gao, M. Y. Vaiman, M. M. Vaiman, and M. Povolotskiy, “N-1-1 ac contingency analysis as a part of nerc compliance studies at midwest iso,” in *IEEE Conference Proceedings*, 2010.
- [7] F. Milano, *Power System Modelling and Scripting*. Springer, 2010.
- [8] S. Juneja and P. Shahabuddin, “Rare-event simulation techniques: An introduction and recent advances,” in *Handbooks in Operations Research and Management Science*, Elsevier, 2006.
- [9] S. Asmussen and P. W. Glynn, *Stochastic Simulation: Algorithms and Analysis*, vol. 57 of *Stochastic Modelling and Applied Probability*. Springer, 2007.
- [10] H. Touchette, “The large deviation approach to statistical mechanics,” *Physics Reports*, vol. 478, no. 1–3, pp. 1–69, 2009.
- [11] G. Rubino and B. Tuffin, *Rare Event Simulation using Monte Carlo Methods*. John Wiley & Sons, 2009.
- [12] M. I. Freidlin and A. D. Wentzell, *Random Perturbations of Dynamical Systems*, vol. 260 of *Grundlehren der mathematischen Wissenschaften*. Springer, 3 ed., 2012.
- [13] C. Hartmann and C. Schütte, “Efficient rare event simulation by optimal nonequilibrium forcing,” *Journal of Statistical Mechanics: Theory and Experiment*, 2012.
- [14] T. Grafke and E. Vanden-Eijnden, “Numerical computation of rare events via large deviation theory,” *Chaos*, 2019.
- [15] I. Dobson, B. A. Carreras, V. E. Lynch, and D. E. Newman, “Complex systems analysis of series of blackouts: Cascading failure, critical points, and self-organization,” *Chaos*, vol. 17, no. 2, 2007.
- [16] M. Chertkov, F. Pan, and M. G. Stepanov, “Predicting failures in power grids: The case of static overloads,” *IEEE Transactions on Smart Grid*, 2010.
- [17] M. Chertkov, F. Pan, M. G. Stepanov, and R. Baldick, “Exact and efficient algorithm to discover extreme stochastic events in wind generation over transmission power grids,” in *IEEE Conference on Decision and Control*, 2011.
- [18] R. Pfitzner, K. Turitsyn, and M. Chertkov, “Statistical classification of cascading failures in power grids,” in *IEEE Power and Energy Society General Meeting*, 2011.
- [19] A. B. Owen, Y. Maximov, and M. Chertkov, “Importance sampling the union of rare events with an application to power systems analysis,” *Electronic Journal of Statistics*, vol. 13, no. 1, pp. 231–254, 2019.
- [20] R. Y. Rubinstein, “Optimization of computer simulation models with rare events,” *European Journal of Operational Research*, vol. 99, pp. 89–112, 1997.
- [21] P.-T. De Boer, D. P. Kroese, S. Mannor, and R. Y. Rubinstein, “A tutorial on the cross-entropy method,” *Annals of Operations Research*, 2005.
- [22] A. B. Owen, “Monte carlo theory, methods and examples,” 2013. Online book/notes.
- [23] A. R. Bergen, *Power Systems Analysis*. Pearson Education India, 2009.
- [24] V. Singh, T. Mogeri, and D. Jena, “Uncertainty handling techniques in power systems: A critical review,” *Electric Power Systems Research*, 2022.
- [25] M. Amin, “Energy infrastructure defense systems,” *Proceedings of the IEEE*, 2005.
- [26] S. H. Horowitz, A. G. Phadke, and C. F. Henville, *Power System Relaying*. John Wiley & Sons, 2022.
- [27] M. Wächter, P. Milan, M. Rohden, and J. Peinke, “Stochastic power grid dynamics with renewable sources,” *Physical Review E*, 2015.
- [28] G. Barrera, E. Bjarkason, and S. Hafstein, “The stability of the multivariate geometric brownian motion as a bilinear matrix inequality problem,” *SIAM Journal on Applied Dynamical Systems*, 2025.
- [29] F. Herzog, “Stochastic differential equations,” 2013. Lecture notes.
- [30] L. Pagnier and P. Jacquod, “Optimal placement of inertia and primary control: A matrix perturbation theory approach,” *IEEE Access*, vol. 7, pp. 145889–145900, 2019.
- [31] R. Christie, “Power systems test case archive: 118 bus power flow test case,” 1993. Online resource.
- [32] P. Dagum, R. Karp, M. Luby, and S. Ross, “An optimal algorithm for monte carlo estimation,” *SIAM Journal on Computing*, 2000.